IEEE Access
Multidisciplinary | Rapid Review | Open Access Journal

Received 6 April 2023, accepted 17 April 2023, date of publication 27 April 2023, date of current version 12 May 2023.

Digital Object Identifier 10.1109/ACCESS.2023.3271011

APPLIED RESEARCH

Wound Care: Wound Management System

B. K. SHREYAMSHA KUMAR[1], (Member, IEEE), K. C. ANANDAKRISHAN[1], MANISH SUMANT[2], AND SRINIVASAN JAYARAMAN[3], (Member, IEEE)

[1]TCS Research, Business Transformation Group, Digital Medicine and Medical Technology Unit, TATA Consultancy Services, Bengaluru 560066, India
[2]Business Transformation Group, Digital Medicine and Medical Technology Unit, TATA Consultancy Services, Cincinnati, OH 45241, USA
[3]TCS Research, Business Transformation Group, Digital Medicine and Medical Technology Unit, TATA Consultancy Services, Cincinnati, OH 45241, USA

Corresponding author: Srinivasan Jayaraman (srinivasa.j@tcs.com)

This research was supported by the TCS Internal funding. The funder has no role in the decision to submit the work for publication and the views expressed herein are authors only. The authors acknowledge the HPC–TCS B&TS team for providing us with the ultra-modern HPC infrastructure, which accelerated and supported this work immensely.

ABSTRACT Wound care is a critical aspect of healthcare that involves treating and managing various types of wounds, typically caused by injuries, surgery, or chronic diseases such as diabetes. Chronic wounds can be particularly challenging to manage and often require 3 to 6 months of long-term care. In a few instances, healing durations are highly unpredictable and can vary depending on the severity of the wound, the patient's overall health, and other factors such as medication, nutrition, age, comorbidity, environment, etiology, and immune system function. A chronic wound can significantly impact the quality of life, causing pain, discomfort, limited mobility, higher healthcare cost, and even mortality in severe cases. Effective wound care is crucial for promoting complete and timely healing and reducing the risk of complications that may lead to amputation, infection, and other potentially life-threatening outcomes. This work aims to develop a system that automizes to determine the wound boundaries leveraging the DeepLabV3+SE, measures the wound characteristics such as size and area, and wound shape using a pipeline of morphological operations and connected component analysis modules. The proposed system's performance was evaluated using the publicly available dataset. Results demonstrate that the DeepLabV3+SE has outperformed with significantly high dice and IOU scores of 0.923 and 0.924, respectively, compared with several state-of-the-art methods.

INDEX TERMS Connected component analysis, DeepLabV3+SE, morphological operator, squeeze and excite, wound assessment, wound care.

I. INTRODUCTION

The quality of life in millions of people worldwide have significantly reduced as they suffer from acute and chronic non-healing wounds [1]. The periodic examination and effective treatment of the wounds are crucial for complete and early wound recovery [2]. Ignoring this will result in severe complications like limb amputations and death [3], [4]. Also, the phases of healing in chronic wounds do not progress in an orderly and prompt manner resulting in hospitalization and requiring additional treatment, thereby increasing the cost of health care services annually. This cost in the United States alone was estimated to be around $96.8B [3]. Given this, developing a wound management system has become essential for chronic wound treatment.

The associate editor coordinating the review of this manuscript and approving it for publication was Bing Li.

A fundamental metric for a wound management system is wound quantification, whose accuracy influences the diagnosis and effective treatment by the healthcare professionals [5], [6]. Several research findings have highlighted the importance of wound measurement that aids in evaluating the healing trajectory, evaluating the effectiveness of the treatments, and finding the future treatment plan for the patients, to name a few [7], [8], [9]. Specifically, the wound area measurement provides an effective and reliable predictor of complete wound healing [9] process, like rate of closure, time of closure, and other insights. Usually, most healthcare professionals employ visual assessment or 1D techniques like a ruler, flexible ruler, or adhesive methods that hurt patients due to infection risks and discomfort [5], [10]. This manual process could be more precise, but it is time-consuming, and prone to intra-varability. The above issues could be overcome through standardization. The first

aspect of standardization is wound digitization, followed by wound segmentation and quantification. The second aspect is automatization by exploiting image processing and computer vision techniques paired with artificial intelligence (A.I.) to monitor wound healing at affordable prices continuously. Covid-19 pandemic-fueled growth pushes the healthcare sectors towards digitization. However, due to the complexities involved in the wound digitization process, such as variable lighting conditions and time constraints in clinical laboratories [11], wound segmentation is still a demanding issue.

Currently, a few commercial products like Planimator app [12], Visitrak device [13], and Silhouette Mobile devices [14] are available that capture the wound image using a dedicated camera system with an in-built algorithm for wound assessment. However, these specialized system faces the following challenges: a) Affordability—not all clinics have access due to its cost, b) In-patient visit—still demands the patient's visit to the clinic; and c) Accuracy—measurements are sporadic in nature. Theoretically, various research groups have attempted to solve the segmentation issue through special sessions like the Foot Ulcer challenge or self—initiated wound segmentation work. Based on the technical adoption aspect, wound segmentation can be categorized into traditional [15], [16], [17], [18], [19] and deep learning(DL) approaches [20], [21], [22], [23], [24], [25], [26], [27], [28], [29], [30]. The first category focuses on combining image processing techniques with or without machine learning approaches via hand-crafted features on wound images. Song and Sacan [19] used the Multi-Layer Perceptron (MLP) and a Radial Basis Function (RBF) neural network for the identification of wound region. Hani et al. [15] generated hemoglobin-based images by applying an Independent Component Analysis (ICA) algorithm on the pre-processed RGB images. The generated images segment the granulation tissue from the wound images using K-means clustering. The granulation tissue growth on the wound bed is used to assess the early stages of wound healing. Hettiarachchi et al. [16] applied energy minimizing discrete dynamic contour algorithm on the saturation plane of hue-saturation-value (HSV) color space of the image. Then the enclosed contour is flood filled to estimate the wound area. Fauzi et al. [17] used a modified HSV color space input image and generated a Red-Yellow-Black-White probability map, which aided the segmentation process. The 3D transformation approach attempted by Liu et al. [18] for wound measurement using an integrated approach of structure from motion (SFM) and least squares conformal mapping (LSCM). In general, image processing—based wound segmentation has bottlenecks such as: i) Features parameter depends on the user or expertise experience. So, they are prone to inter and intra-variabilities, ii) the hand-crafted features are affected by illumination, image resolution, skin pigmentation, camera angle, and so, and iii) they are not immune to severe pathologies and rare cases that are very impractical from a clinical perspective [20], resulting in an inferior performance for the hand-crafted feature approach.

Unlike traditional machine learning and image processing-based methods, which make decisions based on hand-crafted features, the DL-based methods combine feature extraction and decision-making. The superior performance of AlexNet [31] on ImageNet classification has created much traction among the research community, including but not limited to semantic segmentation [32], [33], and medical image analysis [34]. Wang et al. [35] used the vanilla fully convolutional neural network (FCN) architecture [32] to estimate the wound area by segmenting the wounds. Then, the estimated wound areas and the corresponding images are considered time-series data to predict the wound healing progress using a Gaussian regression function model. Goyal et al. [36] employed the FCN-16 architecture to classify the pixels, whether it belongs to the wound or not, resulting in a wound segmentation. Liu et al. [37] study attempted to replace vanilla FCN decoder with a skip-layer concatenation up-sampled with bilinear interpolation and appended pixel-wise softmax layer at the last layer to get the segmented image. Lu et al. [38] proposed a color correction and convolutional neural network (CNN) model with a two-step pre-processing pipeline to segment the overall wound without tissue segmentation. Zahia et al. [24] proposed a CNN-based model for tissue segmentation of pressure injury wounds with the help of manual pre-processing steps. Godeiro et al. [39] proposed a watershed algorithm for wound segmentation and explored different CNN architectures like U-Net, Seg-Net, FCN8, and FCN32, for the wound tissue classification. Goyal et al. [26] proposed a diabetic foot ulcer network (DFUNet) to classify healthy skin versus diabetic foot ulcers. Shenoy et al. [27] proposed a deep wound algorithm using CNN to classify nine different wound images. Pholberdee [23] proposed a DL and data augmentation model to segment each wound tissue separately. Cui et al. [28] proposed a CNN for diabetic wound segmentation and probability maps to remove artifacts. Alzubaidi et al. [29] proposed a CNN-based DFU_QUTNet to classify diabetic foot ulcers versus healthy skin from RGB color images. Chino et al. [30] proposed an automatic skin ulcer assessment framework for accurate wound segmentation and measurement. Sarp et al. [25] proposed a hybrid wound segmentation and tissue classification algorithm by exploiting the conditional generative adversarial network (cGAN) to learn directly from data without human knowledge. Scebba et al. [21] proposed a detect-and-segment algorithm to produce wound segmentation maps with high generalization capabilities. Anisuzzaman et al. [22] presented an automated wound localizer based on the YOLOv3 model followed by segmentation and classification.

Even though the DL approaches have improved the performance of wound segmentation to some extent, the complexities involved in the wound digitization process instruct greater number of DL model parameters to accurately analyze the wound images. Furthermore, there exists a gap

in estimating the wound parameters such as shape, length, width, perimeter, circle diameter, for analyzing the wound, which plays a crucial role in therapy. In addition, there is no complete wound management system integrated with the human-in-the-loop (HIL) module, as per the author's knowledge, which is one of the motivations of this work. Considering the above facts, developing a robust system that tackles these challenges is essential.

Our proposed system has the following technical contributions: 1)

1) The complete wound management system framework consists of patient and physician portals that amalgamate personal information with clinical parameters.
   a) Each module for the proposed system has been implemented as an API for easy integration with the existing electronic medical records (EMR), electronic health records (EHR), or a standalone system.
   b) From the security aspect, in the proposed system, the wound data access has been authenticated using JSON Web Token (JWT) and further the dataset is encoded with the received JWT and stored in the cloud environment.
2) The state-of-the-art DeepLabV3+ algorithm combined with the Squeeze and Excite (SE) network leverages to determine the multiple wound boundaries effectively; for a given single image with multiple wounds.
3) Wound assessment module has been applied in the pipeline to provide high-fidelity wound metrics or attributes along with wound shape estimation, which eases the physician's workload toward understanding the wound progression.
4) Self-learning of the DL module has been powered by the human-in-the-loop approach using the interactive GrabCut algorithm.

The rest of the paper is organized in the following way. Section− II explains the wound management system, and section− III presents the system's outcome and briefly discusses the findings. Section− IV explains the system's limitations, and finally, we conclude this work with our future focus in section− V.

II. METHODOLOGY

A. WOUND MANAGEMENT SYSTEM'S OVERVIEW

The proposed wound management system (WMS) is designed to assist the Physician / Health Care worker in diagnosing and treating wounds. WMS system consists of three (3) stakeholders, a) the Patient, b) the Healthcare provider, and c) the Physician, as shown in Fig. 1. In the WMS pipeline, the mobile phone is utilized for gathering wound images, referred to as the patient portal. After de-identification, captured wound images will get securely uploaded to a dedicated healthcare provider cloud platform for further analysis. Physician portal uses two-way communication, i.e., to get wound assessment results and to provide feedback on the outcome (human-in-the-loop).

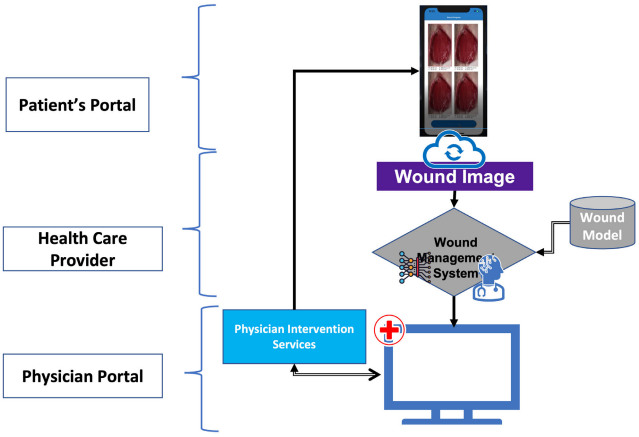

FIGURE 1. Functional block diagram representation of wound management system with human-in-the-loop approach.

Fig. 2 shows the Wound Management system and its pipeline components. Here, the patient portal is a user-friendly mobile application for Android / iOS devices and captures wound images using a mobile camera. Meta data like Patient-ID, Patient-Name, time/date stamp, wound event, and region tagging by the patient are attached with the wound images to create a patient record or dataset. The individual patient record is also stored locally in JSON format, thus allowing the patient to add images to the existing wound event and region tagging. Images changed since the last upload are filtered and periodically prepared for subsequent upload to the cloud server.

Connection to the healthcare provider cloud platform follows OAuth standard and uses a JSON Web Token (JWT) for authorized data transfer. The patient record comprising wound image and meta-data is encoded with the received JWT and uploaded to the cloud portal via Rest API using TLS (transport layer security) encryption. For feedback, the application displays a chart of wound area Vs time and few parameters after the Physician's analysis, which will be explained in detail at the result section III.

The Physician portal is the centerpiece, where the wound images are analyzed using DL and wound assessment (WA) modules implemented in a cloud platform. The Physician portal shows the patient details, wound image, and the analyzed wound image with wound metrics and shape overlaid on the wound image. The Physician portal exhibits the wound measurements such as area, perimeter, and healing index obtained from the WA module in a chart form for diagnosis. Also, it displays the medications prescribed by the physician and the wound history by plotting the wound metric over time. The Physician portal has two components:

1) FRONT-END

It is designed using React Native and can be browser-based or deployed on iPhone/Android phones. This application interacts with the cloud−hosted back-end servers: DL-WA, and Database servers, as described in the Back-end

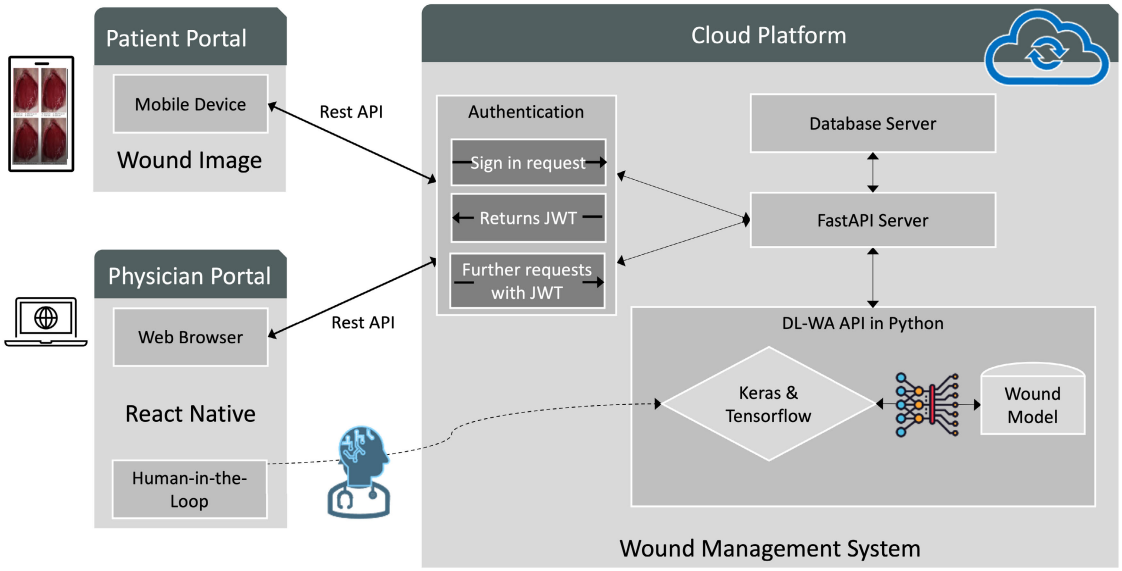

FIGURE 2. Wound management system architecture.

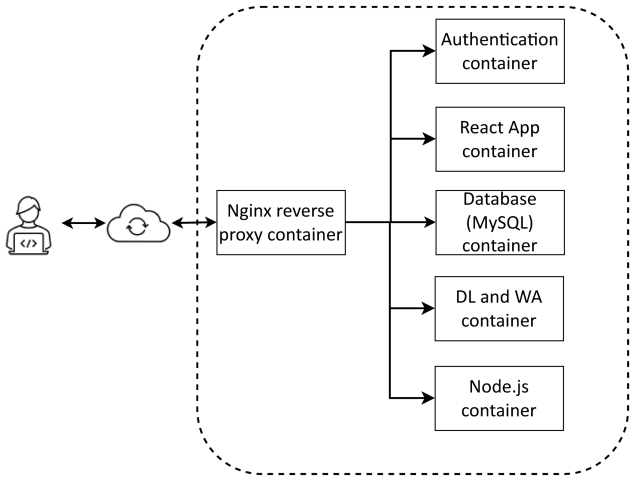

FIGURE 3. Wound management system containerization.

architecture (Fig. 2). These servers are accessed using Rest API. Upon launching the portal front-end, an authorized connection to the back-end servers gets established, and the React application state gets populated with a connection to the Database server. The user interface (UI) design was evaluated for usability in a clinical situation with physician input allowing easy comparison of wound healing progression using actual wound images and charted metrics. A touchscreen-based interactive environment marks the wound areas and backgrounds for the Human-in-the-loop implementation.

2) BACK-END

Sitting behind a Rest API - Database server and DL-WA servers are implemented on a cloud platform using Docker containers, and Nginx reverses proxy as shown in the Fig. 3. After authentication following OAuth standards, secure access to the Rest API is ensured using JWT. The portal interacts with the Database and DL-WA servers via the Rest API. Service on the health care cloud platform is responsible for decoding the dataset and storing received data to an instance of MySQL service. Secure and authorized communication between services is established over the user-defined-bridge network.

3) OPERATIONAL GUIDE

The physician can open a patient record using the Patient ID. Newly uploaded images are available on the Physician portal front end for analysis and review. The physician can also review wound history and patient details relevant to wound diagnosis. Remarks made by the physician and the calculated wound healing metrics are stored in the Database. Additionally, the analyzed images get uploaded to the cloud Database for future review. In addition, the physician can edit the wound annotation boundary, which is feedback to the DL server to complete the human-in-the-loop mechanism.

B. DEEP LEARNING (DL) MODULE

In this work, the DeepLabV3+SE, with Resnet-50 as the encoder, is explored for wound segmentation, and its block diagram is shown in Fig. 4(a). The text in each gray block in Fig. 4(a) represents the number of filters, the kernel size, and a dilation rate of a convolutional layer followed by a batch normalization and a Relu activation function. The final activation function used before the segmentation output is a Sigmoid function. As shown in Fig. 4(a), only two outputs from ''conv2_block3_2_relu'' (denoted as **A**) and ''conv4_block6_2_relu'' (denoted as **B**) layers of the Resnet-50 network are used and hence, only used part of the Resnet-50 architecture as shown in Fig. 4(b). Note that X2,

X3, and X5 mentioned in front of the dotted blocks inside the **conv2_block**, **conv3_block** and **conv4_block** represent the repetitions of the respective dotted blocks by 2, 3 and 5 times, respectively.

In the Resnet-50 encoder, the weights are initialized with the pre-trained weights obtained from the ImageNet dataset. Compared to the random weight initialization, the pre-trained weight initialization converges the model faster with better accuracy, thereby improving the efficiency and generalization ability of the DeepLabV3+SE model. The output of the ''conv4_block6_2_relu'' layer from the Resnet-50 is given to Atrous Spatial Pyramid Pooling (ASPP) [40] consisting of dilated convolutions with different dilation rates that help to encode multi-scale contextual information. ASPP resamples the feature layer with mapping at multiple rates before the convolution layer. This approach efficiently captures the objects and image context with multiple filters and scales.

Further, the output of ASPP is bilinearly up-sampled by a factor of 4 and then concatenated with the output of a convolutional layer of 48 filters with a kernel size of 1×1. The concatenated output is passed through a Squeeze and Excitation (SE) network [41], where the inter-dependencies between channels of the convolutional features are explicitly modeled to improve the representational power of the DeepLabV3+network. In addition, it dynamically re-calibrates the channel-wise features to emphasize informative features and suppress the non-useful ones. The output of the SE network is passed through the two convolutional layers of 256 filters with 3×3 kernel size, followed by another SE network. The output of the second SE network is up-sampled with a bilinear interpolation by a factor of 4. The up-sampled output is passed through a convolutional layer of a single filter with a kernel size of 1×1, followed by a Sigmoid activation function to get the segmentation output.

C. WOUND ASSESSMENT (WA) MODULE

Wound measurement is one of the crucial components in the wound management system, the accuracy of which influences the diagnosis and treatment by healthcare professionals. Also, it is critical to evaluate the wound healing trajectory and determine the future treatment. In addition, the wound area gives an effective and reliable index of later complete wound healing. These functions were accomplished by the WA module that estimates the wound parameters, predicts the wound shape, and overlays the wound metrics on the input image along with the wound boundary. WA module receives the segmented mask generated by the DL module, and it is pre-processed with a threshold value to generate a binary mask, which would be used for further processing. WA module includes morphological operations, connected component analysis, wound parameter estimation, and shape analysis, as shown in Fig. 5.

Morphology operations are performed on the binary mask to remove the tiny regions/spurious noises and to fill the small holes within the wound to improve the true positive rate. In a few cases, the deep learning network could identify the blood stain as a wound, causing a small false-positive region/noise in the segmented mask. This small false-positive region is detected and removed by performing morphological operations on the segmented mask. On the other hand, the abnormal tissue, like fibrinous tissue inside the wound, could be treated as a non-wound region by the network representing it as small holes inside the segmented mask. These holes are detected and filled by morphological operations.

The connected component analysis is acclimated to label the connected regions followed by measurement of those labeled connected regions. The wound metrics, such as area, perimeter, circle diameter, and major and minor axis length of the ellipse, are used in conjunction with the shape analysis algorithm to find the approximate shape of the wound. For example, the eccentricity parameter of ellipse [42], circularity [43], and rectangularity (extent) are adopted in the shape analysis algorithm to determine the wound shape. The eccentricity of ellipse e is calculated using Eq. (1); however, the circle is a particular case when $e = 0$ [42].

$$e = \frac{\text{distance between foci}}{\text{length of major axis}}, \quad 0 \leq e < 1 \tag{1}$$

As the name says, the circularity Ω_c measures the roundness of the shape and is defined by

$$\Omega_c = 4\pi \frac{A}{r^2} \tag{2}$$

where A = Area and r = Perimeter. For a perfect circle $\Omega_c = 1$ [43]. Rectangularity (extent) ψ_R [44] is calculated using Eq. (3).

$$\psi_R = \frac{\text{no. of pixels in ROI}}{\text{no. of pixels in a boundary box}} \tag{3}$$

Based on the values of these parameters, e, Ω_c, and ψ_R, the approximate shape of the wound is determined. Finally, the measured parameters and the wound boundary are overlaid on the wound image.

D. HUMAN-IN-THE-LOOP

Human-in-the-loop has been introduced to improve the system's accuracy and enable the DL module's self-learning feature. In addition, our system will be validated by the physician or user every time they use the tool, which is a double verification process. For example, during the physician's investigation, if the Physician determines that the wound segmentation outcome is inaccurate, he can rectify it via the interactive GrabCut module [45] as shown in Fig. 6. Else Physician approves the segmentation output, and the WA module estimates the wound metrics that are overlaid on the wound image along with the wound boundary for display on the physician portal. As a process of personal information integration, wound segmentation's output with wound metrics and its original wound image are stockpiled in the Database server. On the other hand, when the physician opts for correcting the wound boundary via GrabCut, he annotates the foreground and background,

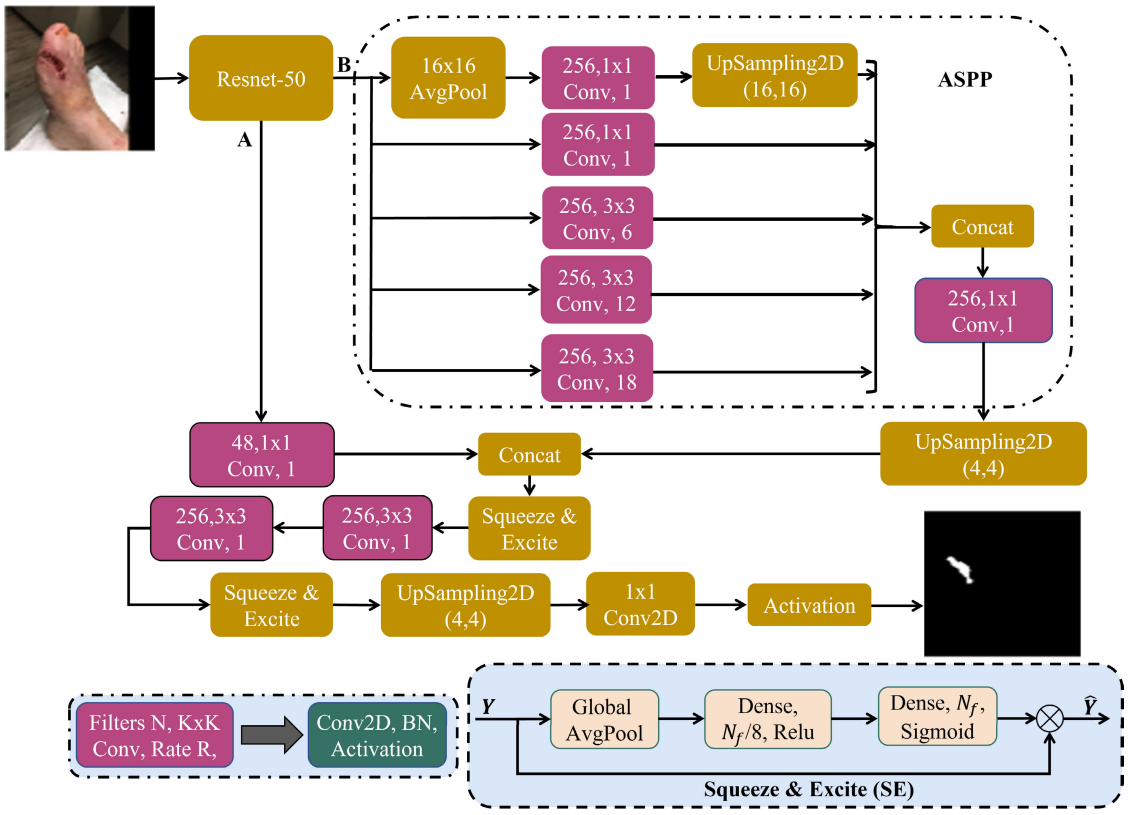

(a) DeepLabV3+SE architecture with Resnet-50 as encoder

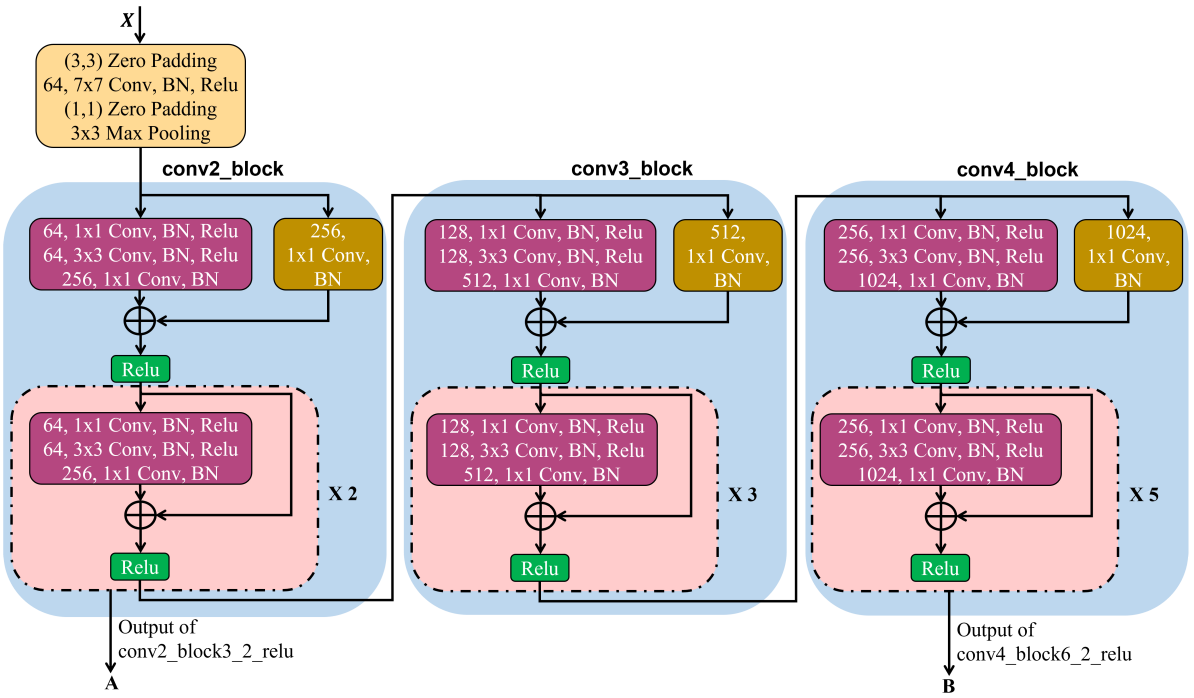

(b) Resnet-50 architecture used as encoder in DeepLabV3+SE

FIGURE 4. Block diagram representation of the DeepLabV3+SE architecture with Resnet-50 as encoder.

and the system extracts the boundaries. The process of annotating the foreground and background is repeated till the Physician is satisfied with the segmented boundary by the GrabCut. The corrected segmentation output and its original wound are accumulated in the server. Once the number of accumulated physician corrected segmented images exceeds

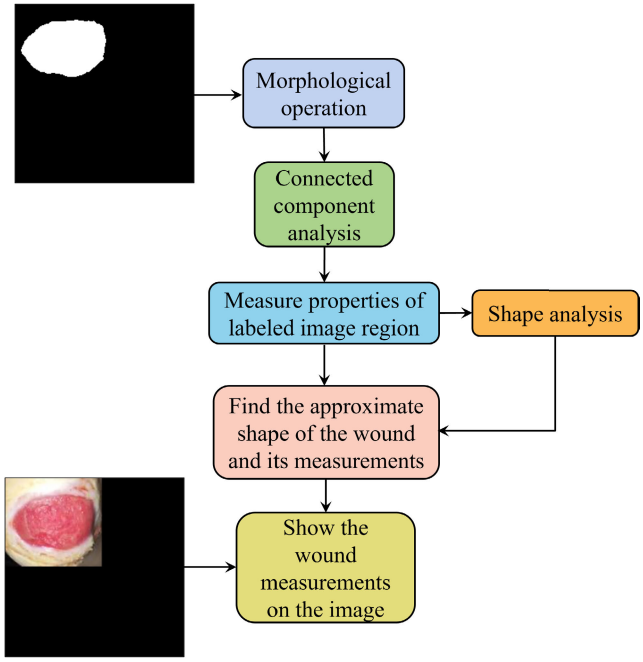

FIGURE 5. Functional block diagram of wound assessment (WA) module that enhances the segmentation outcome of the DeepLabV3+SE, and estimates the wound metrics as well as finds the approximate shape of the wound.

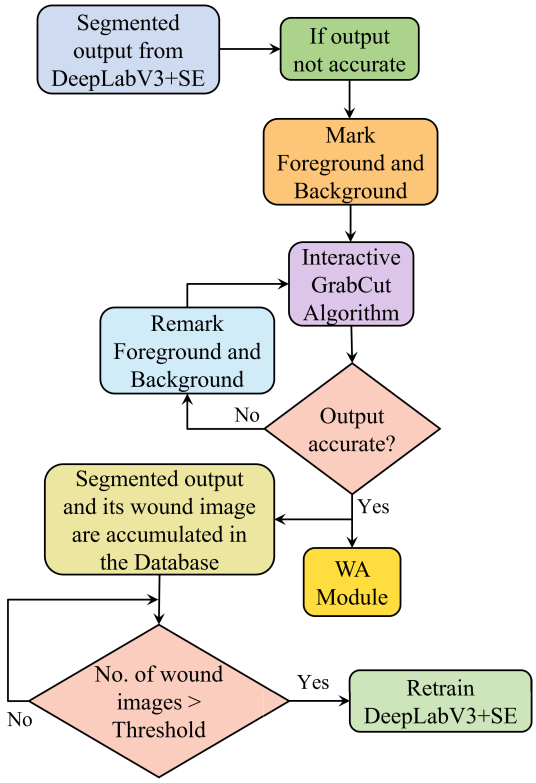

FIGURE 6. Flow diagram of human-in-the-loop.

the set threshold value then the DL module's retraining is initiatied automatically, thereby leveraging the self-learning technique. The accumulated segmentation outputs obtained by the GrabCut with the physician's input will function as the ground truth for retraining, which empower the DL module accuracy.

III. RESULTS AND DISCUSSION

The front-end GUI and workflow of WMS are shown in Fig. 7. The physician can view the patient details and wound history relevant to the wound diagnosis by opening a patient record using a Patient ID. Charts and wound progress section of the Physicians portal, shown in Fig. 7 represents the wound measurement history and the set of wound images, respectively, for making observations about the wound healing progress. The DL and WA modules were implemented in Python with Keras and TensorFlow as back-end and trained and validated on HPC-A3 TCS (TATA Consultancy Services) server powered by NVIDIA DGX-A100 series. The DL and WA modules reside in the API server, and the trained DeepLabV3+ SE model, the patient's information data, and the accumulated segmentation outputs from GrabCut and their respective wound images are stored in the Database server.

A. DATASET

In this work, we have used the publicly available AZH Wound care dataset [46] and the Foot Ulcer Challenge (FUC) Segmentation dataset [46]. Both datasets are merged, which results in a total of 1841 images, and for the homogeneousness aspect, the images are resized to 256×256. Furthermore, the image augmentation techniques, such as brightness and saturation improvement, hue and rotation, cut mix and mixup, and horizontal and vertical flips, were adapted to increase the training dataset from 1675 to 55,275 wound images, which is more extensive than the DFUC2021 challenge dataset [47]. The validation and testing sets had 166 and 278 images, respectively, and have been used without augmentation for validation and testing of the model.

B. MODEL PERFORMANCE EVALUATION METRICS

In this study, the performance was evaluated using the evaluation metrics like Dice Score, Intersection over Union (IoU), Precision, and Recall, which are given below for completeness.

$$Dice\ Score = \frac{2 \times TP}{2 \times TP + FP + FN} \tag{4}$$

$$IOU = \frac{TP}{TP + FP + FN} \tag{5}$$

$$Precision = \frac{TP}{TP + FP} \tag{6}$$

$$Recall = \frac{TP}{TP + FN} \tag{7}$$

C. DL RESULTS

In DL training, the learning rate was initialized as 0.0001, and each mini-batch size of 16 images was adapted, considering

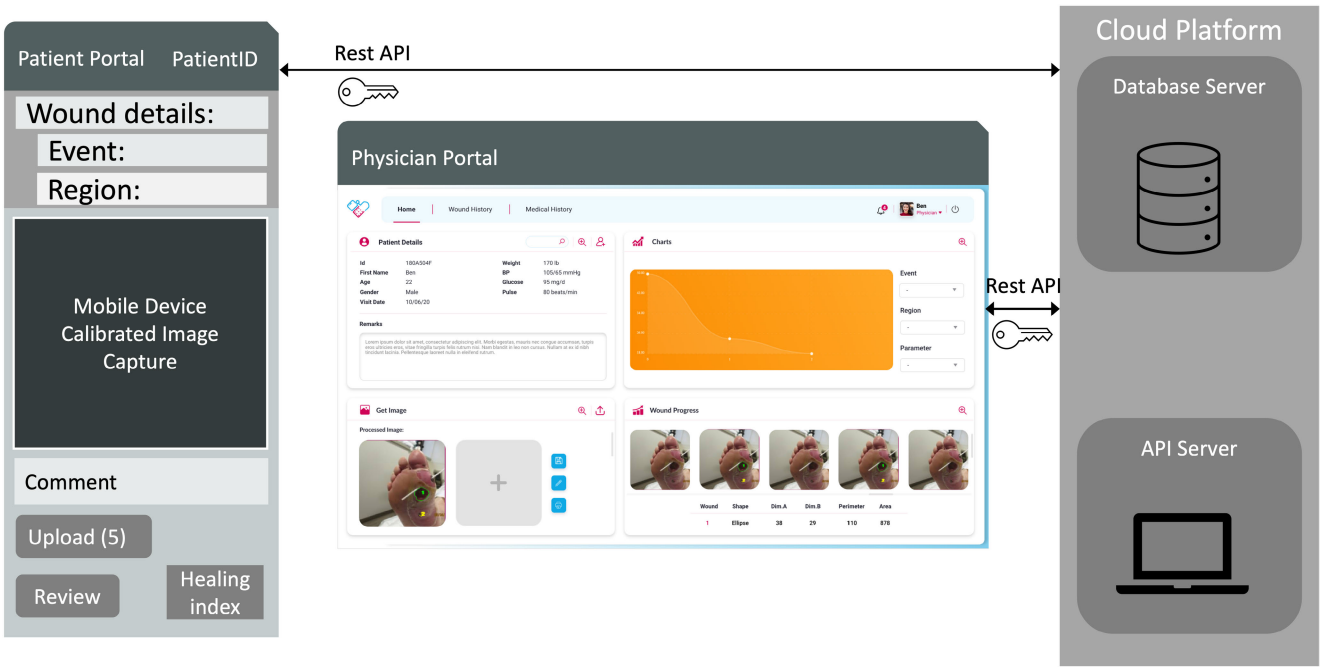

FIGURE 7. Front end GUI and workflow of the wound management system.

the trade-off between the training accuracy and efficiency. On the one hand, training loss quantification infers how well the model fits the training data, and on the other hand, validation loss assesses how well the model fits the new data. In order to have a balanced training by avoiding under-fitting and over-fitting, both losses should be watched during the training. Hence, the training is terminated early when both the losses converged and there was no significant improvement in the validation loss for more than 10 epochs, as shown in Fig. 8. Adam's optimization algorithm was adapted to update the network parameters. The number of trainable parameters of DeepLabV3 and DeepLabV3+ SE with that of other state-of-the-art methods and their performance comparisons in terms of evaluation metrics, Dice, IOU, Precision, and Recall, are given in Table 1. To evaluate the performance of the DL module, the testing set of AZH wound care dataset [46] is used in both DeepLabV3 and DeepLabV3+SE. The number of trainable parameters and evaluation metrics of VGG-16, SegNet, U-Net, Mask-RCNN, MobileNetV2, and MobileNetV2+CCL, and Ensemble of CNNs (ECNN), which are evaluated on the same testing dataset, are reported from [20] and [48], respectively.

The result finding infers that the proposed method (DeepLabV3+SE) outperforms DeepLabV3+, ECNN, MobileNetV2+CCL, MobileNetV2, Mask-RCNN, U-Net, SegNet and VGG16 in the performance measure, the Dice score, by 0.4%, 0.2%, 1.9%, 2.2%, 2.3%, 2.4%, 8.4% and 13.9%, respectively. Similarly, in the second performance metric- IoU, the DeepLabV3+SE outperforms DeepLabV3+ and ECNN by 0.4% and 8.0%, respectively. In terms of Precision, DeepLabV3+SE outperforms

TABLE 1. Evaluation metrics of DeepLabV3+SE with Resnet-50 encoder.

Model	# Params	Dice	IOU	Pre	Recall
VGG16 [20]	134,264,641	0.810	-	0.839	0.783
SegNet [20]	902,561	0.851	-	0.836	0.865
U-Net [20]	4,834,839	0.901	-	0.890	0.913
Mask-RCNN [20]	63,621,918	0.902	-	0.943	0.864
MobileNetV2 [20]	2,141,505	0.903	-	0.908	0.897
MobileNetV2+CCL [20]	2,141,505	0.905	-	0.910	0.899
ECNN [48]	-	0.921	0.855	0.927	**0.918**
DeepLabV3+	11,868,481	0.919	0.920	**0.964**	0.876
DeepLabV3+SE (Proposed)	11,891,585	**0.923**	**0.924**	0.960	0.883

ECNN, MobileNetV2+CCL, MobileNetV2, Mask-RCNN, U-Net, SegNet and VGG16 by 3.5%, 5.5%, 5.7%, 1.8%, 7.8%, 14.8% and 14.4%, respectively, and under-performs DeepLabV3+ by 0.4%. However, DeepLabV3+SE underperforms ECNN, MobileNetV2+CCL, MobileNetV2 and U-Net by 3.8%, 1.7%, 1.5% and 3.3%, respectively, and outperforms DeepLabV3+, Mask-RCNN, SegNet and VGG16 by 0.8%, 2.2%, 2.1% and 12.7%, respectively, in-terms of Recall. Generally, the higher the number of trainable parameters, the better the model's performance. However, it is not so concerning in Mask-RCNN and VGG16, which require 5.5 and 11.3 times higher parameters than DeepLabV3+SE, respectively, and still underperform. On the other hand, SegNet, both MobileNetV2 and MobileNetV2+CCL, and U-Net need 13, 5.5, and 2.4 times lower parameters than DeepLabV3+SE, respectively, and performed better than DeepLabV3+SE, except SegNet, only in terms of Recall. Considering the trade-off between the performance and number of trainable parameters, the proposed DeepLabV3+SE performs better in terms of Dice

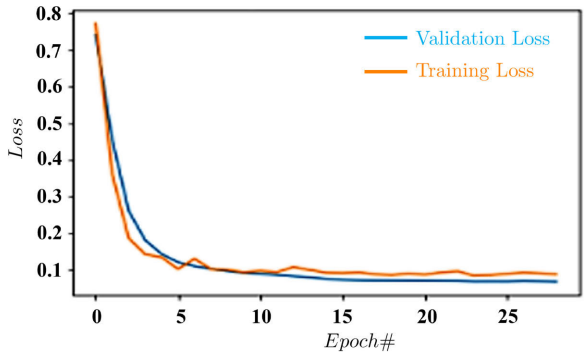

FIGURE 8. Training and validation loss metrics of DeepLabV3+SE.

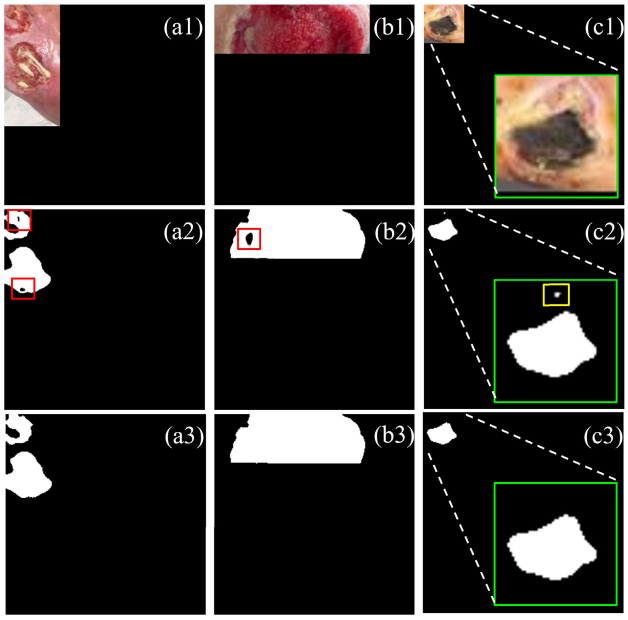

FIGURE 9. Wound Assessment module's segmentation outcome with color code for some test images. Here (a1)-(c1) represents the original image, (a2)-(c2) are the segmented outputs from DeepLabV3+SE, and (a3)-(c3) are the outputs of post-processing. Note that red boxes in (a2) and (b2) show holes, and the yellow box in (c2) depicts spurious noise. The green box in (c1), (c2), and (c3) shows the zoomed wound area and its masks from DeepLabV3+SE and after post-processing, respectively.

and IOU scores than others, regardless of the chronic wound segmentation dataset. Thus, it is evident that our model is robust and unbiased for wound segmentation with a single image that has been captured via a single camera system. Besides this, our system pipeline consists of a WA module to estimate the wound parameters and to find the approximate wound shape from the sequence of DeepLabV3+SE's output images.

D. WOUND ASSESSMENT MODULE RESULTS

The wound images, segmented masks obtained from DeepLabV3+SE, and the respective post-processed outputs are shown in Fig. 9. In Fig. 9, (a1)-(c1) shows the original wound images, (a2)-(c2) shows the segmented masks obtained from DeepLabV3+SE, and (a3)-(c3) shows the

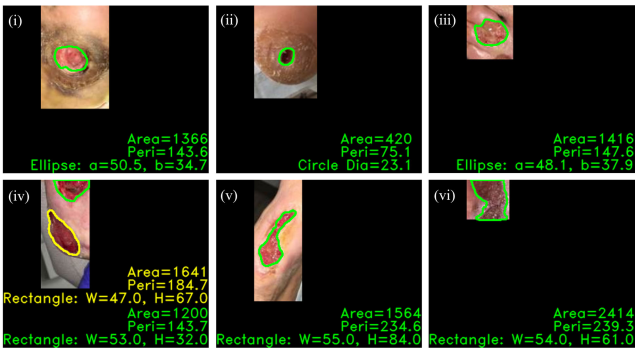

FIGURE 10. Wound Measurements such as area, perimeter, and shape (rectangle, circle, and ellipse) are given with color code visual layout representing the wound boundary for some test images. Green and Yellow color visual layouts represent the first and second wounds in the original wound image, respectively.

outputs after post-processing. The holes in the segmented masks obtained from DeepLabV3+SE are represented with a red box in Fig. 9 (a2) and (b2), and the spurious noise is shown with a yellow box in Fig. 9(c2). These holes and the noises are removed after post-processing, as shown in Fig. 9(a3)-(c3). In Fig. 9 (c1,c2) and (c3), the green boxes represent the zoomed version of the wound image, segmented masks obtained from DeepLabV3+SE, and the post-processed output, respectively, to show the removal of spurious noise. The post-processing carried out after image segmentation in [20] uses only connected component labeling to remove the holes and noises in the wound region and outside the ROI, respectively. In contrast, our method uses morphological operations to remove noises and holes, and the connected component analysis for labeling the wound regions. These labeled connected regions are used for estimating wound dimensions such as width, length, circle diameter, major and minor axis length of the ellipse, area, and perimeter. These measurements are used in conjunction with shape analysis to find the approximate shape of the wound, as shown in Fig. 10 for the test images. In Fig. 10, the wound's nearest shape and its respective parameter measurements are overlaid on the wound image. For example, the wound images (i & iii) in the first row, the wound shape is an ellipse and its parameters, the major axis length (**a**), and minor axis length of the ellipse (**b**) are overlaid along with area and perimeter of the wound. If the approximate wound shape is a rectangle, the width (**W**), height (**H**), area and perimeter are overlaid on the wound image. Similarly, in case of circle shape wound, the diameter, area, and perimeter are indicated for the circular wound image.

E. HUMAN-IN-THE-LOOP RESULTS

The images obtained during the GrabCut process are shown in Fig. 11. This process is interactive and iterative, as shown in Fig. 6, which directly depends on the user's feedback. For example, Fig. 11 (a) and (b) represent the GrabCut annotation process (Foreground and Background marking in Blue and Green colors, respectively) and its corresponding

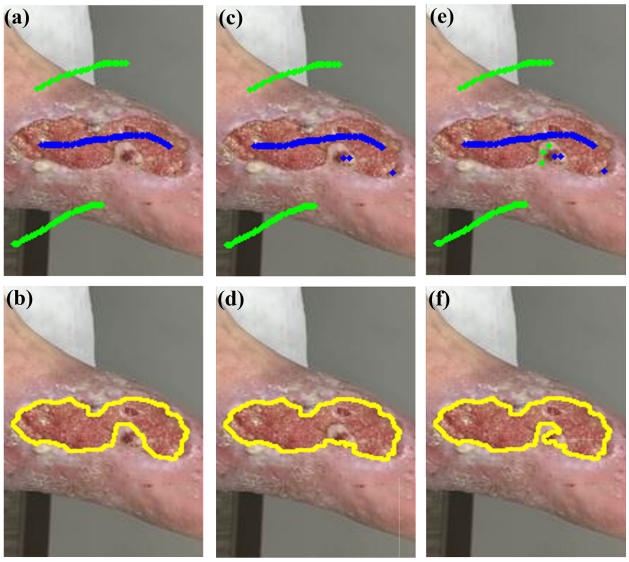

FIGURE 11. Images obtained during the interactive GrabCut. (a), (c) and (e) represent the Images with Foreground and Background markings for 1^{st}, 2^{nd}, and 3^{rd} iterations, respectively. Note that foreground and background are marked with blue and green colors, respectively. (b), (d) and (f) show the original wound image with the boundary marked in Yellow color as an outcome of the GrabCut process.

output. Suppose the user or physician is unsatisfied or neglects a region to annotate, then the next iteration could be repeated as represented in Fig. 11 (c,d), and (e,f), which results in improving the accuracy of the boundary region.

IV. LIMITATION

In this study, due to the privacy concern, the publicly available AZH Wound care [46] and the Foot Ulcer Challenge Segmentation [47] datasets have been used for training the DeepLabV3+SE model. The wound images in these datasets are captured with different image-capturing devices without camera calibration. As the camera was not calibrated during the image capture, the mapping from the digital world in terms of pixels to the physical units is impossible. Due to this limitation, wound measurements are presented in terms of pixels (digital domain) rather than the physical units in Fig. 10. The above limitation could be addressed by calibrating the camera before or while capturing the wound images. Thus, the wound measurements in pixels can be mapped to the real-world physical units using the scaling factor obtained during the camera calibration.

V. CONCLUSION

In this paper, the wound management system using DeepLabV3+SE network for wound segmentation outperformed with a significantly high Dice score and IOU in the automated wound boundary detection. In addendum, quantitative assessment of wound parameters and prediction of the wound shape demonstrates that it generally works well in a diverse environment. HIL module provides input to the self-learning process, i.e., it updates the DeepLabV3+SE model over a period with the help of a physician's feedback. A new model is deployed after retraining whenever the number of segmented images; the Physician corrects surpasses the set threshold value. Thus, our proposed system has the following potential benefits/advantages:

1) Robustness: A single camera system can handle any type of wound images captured in different environments with challenges like uneven illumination, low image resolution, different image shape, skin pigmentation, and so on, that occur individually or in combination.
2) Wound assessment module helps the Physician to understand the progress of the wound and analyze the effect of medication on the wound healing over a period of time. Having all the information on wound metrics and medications at his disposal, he can take the necessary action for faster wound healing.
3) Self-learning of the DL module due to the exploitation of the human-in-the-loop approach improves the accuracy and performance of the system.
4) The proposed telemedicine system will enhance the pervasive wound monitoring and care management strategies for the Physician and the Patient.

Adopting our proposed system in the continuum of care-remote monitoring will enhance the Physician's pervasive wound diagnosis and management strategies, and the patient in a rural area or far-off distance can have access to an early, improved, and cost-effective diagnosis. In future work, we are focus on removing the dependency on masks or annotations by using either semi-supervised or unsupervised networks. In addition, the data security model integration with HIPAA standards compliances will be adopted to complete the system's full functionality.

ACKNOWLEDGMENT

The funder has no role in the decision to submit the work for publication and the views expressed herein are authors only. The authors acknowledge the HPC-TCS B&TS team for providing them with the ultra-modern HPC infrastructure, which accelerated and supported this work immensely.

REFERENCES

[1] R. G. Frykberg and J. Banks, "Challenges in the treatment of chronic wounds," *Adv. Wound Care*, vol. 4, no. 9, pp. 560–582, Sep. 2015.
[2] G. Han and R. Ceilley, "Chronic wound healing: A review of current management and treatments," *Adv. Therapy*, vol. 34, no. 3, pp. 599–610, Mar. 2017.
[3] C. K. Sen, "Human wounds and its burden: An updated compendium of estimates," *Adv. Wound Care*, vol. 8, no. 2, pp. 39–48, Feb. 2019.
[4] J. Escandon, A. C. Vivas, J. Tang, K. J. Rowland, and R. S. Kirsner, "High mortality in patients with chronic wounds," *Wound Repair Regeneration*, vol. 19, no. 4, pp. 526–528, Jul. 2011.
[5] L. A. Lavery, S. A. Barnes, M. S. Keith, J. W. Seaman, and D. G. Armstrong, "Prediction of healing for postoperative diabetic foot wounds based on early wound area progression," *Diabetes Care*, vol. 31, no. 1, pp. 26–29, Jan. 2008.

[6] S. Coerper, S. Beckert, M. A. Küper, M. Jekov, and A. Königsrainer, "Fifty percent area reduction after 4 weeks of treatment is a reliable indicator for healing—analysis of a single-center cohort of 704 diabetic patients," *J. Diabetes Complications*, vol. 23, no. 1, pp. 49–53, 2009.

[7] K. Ousey and L. Cook, "Understanding the importance of holistic wound assessment," *Pract. Nursing*, vol. 22, no. 6, pp. 308–314, Jun. 2011.

[8] L. Russell, "The importance of wound documentation and classification," *Brit. J. Nursing*, vol. 8, no. 20, pp. 1342–1354, Nov. 1999.

[9] M. Cardinal, D. E. Eisenbud, T. Phillips, and K. Harding, "Early healing rates and wound area measurements are reliable predictors of later complete wound closure," *Wound Repair Regener.*, vol. 16, no. 1, pp. 19–22, Jan. 2008.

[10] K. L. Wu, K. Maselli, A. Howell, D. Gerber, E. Wilson, P. Cheng, P. C. Kim, and O. Guler, "Feasibility of 3D structure sensing for accurate assessment of chronic wound dimensions," *Int. J. Comput. Assist. Radiol. Surg.*, vol. 10, no. 1, pp. 13–14, 2015.

[11] C. P. Loizou, T. Kasparis, and M. Polyviou, "Evaluation of wound healing process based on texture image analysis," *J. Biomed. Graph. Comput.*, vol. 3, no. 3, pp. 1–13, Mar. 2013.

[12] P. Foltynski, "Ways to increase precision and accuracy of wound area measurement using smart devices: Advanced app planimator," *PLoS ONE*, vol. 13, no. 3, Mar. 2018, Art. no. e0192485, doi: 10.1371/journal.pone.0192485.

[13] S. Treuillet, B. Albouy, and Y. Lucas, "Three-dimensional assessment of skin wounds using a standard digital camera," *IEEE Trans. Med. Imag.*, vol. 28, no. 5, pp. 752–762, May 2009.

[14] U. Pavlovčič, J. Diaci, J. Možina, and M. Jezeršek, "Wound perimeter, area, and volume measurement based on laser 3D and color acquisition," *Biomed. Eng. OnLine*, vol. 14, no. 1, p. 39, Dec. 2015.

[15] A. F. M. Hani, L. Arshad, A. S. Malik, A. Jamil, and F. Y. B. Bin, "Haemoglobin distribution in ulcers for healing assessment," in *Proc. 4th Int. Conf. Intell. Adv. Syst. (ICIAS)*, Jun. 2012, pp. 362–367.

[16] N. D. J. Hettiarachchi, R. B. H. Mahindaratne, G. D. C. Mendis, H. T. Nanayakkara, and N. D. Nanayakkara, "Mobile based wound measurement," in *Proc. IEEE Point Care Healthcare Technol. (PHT)*, Jan. 2013, pp. 298–301.

[17] M. F. A. Fauzi, I. Khansa, K. Catignani, G. Gordillo, C. K. Sen, and M. N. Gurcan, "Computerized segmentation and measurement of chronic wound images," *Comput. Biol. Med.*, vol. 60, pp. 74–85, May 2015.

[18] C. Liu, X. Fan, Z. Guo, Z. Mo, E. I.-C. Chang, and Y. Xu, "Wound area measurement with 3D transformation and smartphone images," *BMC Bioinf.*, vol. 20, no. 1, pp. 1–21, Dec. 2019.

[19] B. Song and A. Sacan, "Automated wound identification system based on image segmentation and artificial neural networks," in *Proc. IEEE Int. Conf. Bioinf. Biomed.*, Oct. 2012, pp. 1–4.

[20] C. Wang, D. M. Anisuzzaman, V. Williamson, M. K. Dhar, B. Rostami, J. Niezgoda, S. Gopalakrishnan, and Z. Yu, "Fully automatic wound segmentation with deep convolutional neural networks," *Sci. Rep.*, vol. 10, no. 1, Dec. 2020, Art. no. 21897.

[21] G. Scebba, J. Zhang, S. Catanzaro, C. Mihai, O. Distler, M. Berli, and W. Karlen, "Detect-and-segment: A deep learning approach to automate wound image segmentation," *Informat. Med. Unlocked*, vol. 29, 2022, Art. no. 100884.

[22] D. M. Anisuzzaman, Y. Patel, J. A. Niezgoda, S. Gopalakrishnan, and Z. Yu, "A mobile app for wound localization using deep learning," *IEEE Access*, vol. 10, pp. 61398–61409, 2022.

[23] N. Pholberdee, "Wound-region segmentation from image by using deep learning and various data augmentation methods," M.S. thesis, Dept. Comput. Sci., Silpakorn Univ., Pakkret, Thailand, 2019.

[24] S. Zahia, D. Sierra-Sosa, B. Garcia-Zapirain, and A. Elmaghraby, "Tissue classification and segmentation of pressure injuries using convolutional neural networks," *Comput. Methods Programs Biomed.*, vol. 159, pp. 51–58, Jun. 2018.

[25] S. Sarp, M. Kuzlu, M. Pipattanasomporn, and O. Guler, "Simultaneous wound border segmentation and tissue classification using a conditional generative adversarial network," *J. Eng.*, vol. 2021, no. 3, pp. 125–134, Mar. 2021.

[26] M. Goyal, N. D. Reeves, A. K. Davison, S. Rajbhandari, J. Spragg, and M. H. Yap, "DFUNet: Convolutional neural networks for diabetic foot ulcer classification," *IEEE Trans. Emerg. Topics Comput. Intell.*, vol. 4, no. 5, pp. 728–739, Oct. 2020.

[27] V. N. Shenoy, E. Foster, L. Aalami, B. Majeed, and O. Aalami, "Deepwound: Automated postoperative wound assessment and surgical site surveillance through convolutional neural networks," in *Proc. IEEE Int. Conf. Bioinf. Biomed. (BIBM)*, Dec. 2018, pp. 1017–1021.

[28] C. Cui, K. Thurnhofer-Hemsi, R. Soroushmehr, A. Mishra, J. Gryak, E. Dominguez, K. Najarian, and E. Lopez-Rubio, "Diabetic wound segmentation using convolutional neural networks," in *Proc. 41st Annu. Int. Conf. IEEE Eng. Med. Biol. Soc. (EMBC)*, Jul. 2019, pp. 1002–1005.

[29] L. Alzubaidi, M. A. Fadhel, S. R. Oleiwi, O. Al-Shamma, and J. Zhang, "DFU_QUTNet: Diabetic foot ulcer classification using novel deep convolutional neural network," *Multimedia Tools Appl.*, vol. 79, nos. 21–22, pp. 15655–15677, Jun. 2020.

[30] D. Y. T. Chino, L. C. Scabora, M. T. Cazzolato, A. E. S. Jorge, C. Traina-Jr, and A. J. M. Traina, "Segmenting skin ulcers and measuring the wound area using deep convolutional networks," *Comput. Methods Programs Biomed.*, vol. 191, Jul. 2020, Art. no. 105376.

[31] A. Krizhevsky, I. Sutskever, and G. E. Hinton, "ImageNet classification with deep convolutional neural networks," in *Proc. Adv. Neural Inf. Process. Syst.*, 2012, pp. 1097–1105.

[32] J. Long, E. Shelhamer, and T. Darrell, "Fully convolutional networks for semantic segmentation," in *Proc. IEEE Conf. Comput. Vis. Pattern Recognit. (CVPR)*, Jun. 2015, pp. 3431–3440.

[33] A. Garcia-Garcia, S. Orts-Escolano, S. Oprea, V. Villena-Martinez, and J. Garcia-Rodriguez, "A review on deep learning techniques applied to semantic segmentation," 2017, *arXiv:1704.06857*.

[34] G. Litjens, T. Kooi, B. E. Bejnordi, A. A. A. Setio, F. Ciompi, M. Ghafoorian, J. A. W. M. van der Laak, B. van Ginneken, and C. I. Sánchez, "A survey on deep learning in medical image analysis," *Med. Image Anal.*, vol. 42, pp. 60–88, Dec. 2017.

[35] C. Wang, X. Yan, M. Smith, K. Kochhar, M. Rubin, S. M. Warren, J. Wrobel, and H. Lee, "A unified framework for automatic wound segmentation and analysis with deep convolutional neural networks," in *Proc. 37th Annu. Int. Conf. IEEE Eng. Med. Biol. Soc. (EMBC)*, Aug. 2015, pp. 2415–2418.

[36] M. Goyal, M. H. Yap, N. D. Reeves, S. Rajbhandari, and J. Spragg, "Fully convolutional networks for diabetic foot ulcer segmentation," in *Proc. IEEE Int. Conf. Syst., Man, Cybern. (SMC)*, Oct. 2017, pp. 618–623.

[37] X. Liu, C. Wang, F. Li, X. Zhao, E. Zhu, and Y. Peng, "A framework of wound segmentation based on deep convolutional networks," in *Proc. 10th Int. Congr. Image Signal Process., Biomed. Eng. Informat. (CISP-BMEI)*, Oct. 2017, pp. 1–7.

[38] H. Lu, B. Li, J. Zhu, Y. Li, Y. Li, X. Xu, L. He, X. Li, J. Li, and S. Serikawa, "Wound intensity correction and segmentation with convolutional neural networks," *Concurrency Comput., Pract. Exper.*, vol. 29, no. 6, Mar. 2017, Art. no. e3927.

[39] V. Godeiro, J. S. Neto, B. Carvalho, B. Santana, J. Ferraz, and R. Gama, "Chronic wound tissue classification using convolutional networks and color space reduction," in *Proc. IEEE 28th Int. Workshop Mach. Learn. Signal Process. (MLSP)*, Sep. 2018, pp. 1–6.

[40] L.-C. Chen, G. Papandreou, I. Kokkinos, K. Murphy, and A. L. Yuille, "DeepLab: Semantic image segmentation with deep convolutional nets, atrous convolution, and fully connected CRFs," *IEEE Trans. Pattern Anal. Mach. Intell.*, vol. 40, no. 4, pp. 834–848, Apr. 2018.

[41] J. Hu, L. Shen, and G. Sun, "Squeeze-and-excitation networks," in *Proc. IEEE/CVF Conf. Comput. Vis. Pattern Recognit.*, Jun. 2018, pp. 7132–7141.

[42] C. A. Kluever, *Spaceflight Mechanics, Encyclopedia of Physical Science and Technology*. New York, NY, USA: Academic, 2003.

[43] L. Sun, *Structural Behavior of Asphalt Pavements*. Oxford, U.K.: Butterworth-Heinemann, 2016.

[44] Scikit-Image. *Scikit-Image Library*. [Online]. Available: https://scikit-image.org/docs/stable/api/skimage.measure.html

[45] C. Rother, V. Kolmogorov, and A. Blake, "GrabCut: Interactive foreground extraction using iterated graph cuts," in *Proc. ACM SIGGRAPH Papers*, 2004, pp. 309–314.

[46] GitHub. (2020). *Github Repository*. [Online]. Available: https://github.com/uwm-bigdata/wound-segmentation

[47] B. Cassidy, C. Kendrick, N. D. Reeves, J. M. Pappachan, C. O'Shea, D. G. Armstrong, and M. H. Yap, "Diabetic foot ulcer grand challenge 2021: Evaluation and summary," in *Diabetic Foot Ulcers Grand Challenge*. Germany: Springer, 2021, pp. 90–105.

[48] A. Mahbod, G. Schaefer, R. Ecker, and I. Ellinger, "Automatic foot ulcer segmentation using an ensemble of convolutional neural networks," in *Proc. 26th Int. Conf. Pattern Recognit. (ICPR)*, Aug. 2022, pp. 1–6.

B. K. SHREYAMSHA KUMAR (Member, IEEE) received the B.E. degree in electronics and communication engineering from Bangalore University, Karnataka, India, in 2000, and the M.Tech. degree in industrial electronics from the National Institute of Technology Karnataka, Surathkal, Karnataka, in 2004, and the Ph.D. degree in electrical and computer engineering from Concordia University, Montreal, QC, Canada, in 2019.

From 2004 to 2012, he was with the Central Research Laboratory (A Corporate Research Facility of Bharat Electronics), Bengaluru, India, as a member of Research Staff. From 2012 to 2019, he was a Research Associate with the Signal Processing Group, Department of Electrical and Computer Engineering, Gina Cody School of Engineering and Computer Science, Concordia University. He is currently with the Business Transformation Group, Digital Medicine and Medical Technology Unit, TATA Consultancy Services, as a Scientist. He has published several articles in peer-reviewed journals and major conferences. His research interests include computer vision, visual tracking, image fusion, image denoising, image encryption, medical image processing, and document image processing.

Dr. Shreyamsha Kumar was a recipient of the Research and Development Excellence Award by Bharat Electronics, India. He was a team member of a project, which received the Raksha Mantri's Award for Excellence in ''Innovation'' category from Hon'ble Raksha Mantri, Ministry of Defence, Government of India, for the period 2008–2009 on November 2010. He was a recipient of several awards from Concordia University and the high-status Doctoral Research Merit Scholarship for Foreign Students from Ministére de l'Éducation, de l'Enseignement Supérieur et de la Recherche (MEESR) du Québec, during his doctoral studies at Concordia University. He has served as a reviewer for several journals and major conferences.

K. C. ANANDAKRISHAN is currently pursuing the Ph.D. degree in computer science with Amritha Vishwavidyapeetham, Coimbatore. He is a Machine Learning Solution Architect with TATA Consultancy Services.

MANISH SUMANT received the M.S. degree in biomedical engineering from Washington University, St. Louis, in 1995. He has worked on medical device development focusing on software technologies for embedded devices, diagnostic software, and cloud-based solutions. He has a proven record of implementing research technologies and algorithms into innovative solutions. Currently, he is a Solutions Architect with the Digital Medicine and Medical Technologies Unit, TCS.

SRINIVASAN JAYARAMAN (Member, IEEE) is the Principal Scientist and the Head of the Biocomputational and Imaging Program, TCS Research, Digital Medicine and Medical Technologies Unit, BTG, Cincinnati, USA. During his sabbatical, he was a Visiting Scholar with MCCHE, Desautels Faculty of Management, McGill University, Montreal, Canada, in July 2017; a Research Fellow with Énergie Matériaux Télécommunications Research Centre (NRS-EMT), Montreal, in July 2016; and a Postdoctoral Fellow (Scientific Manager) with the University of Nebraska Lincoln (ULN), USA, and the New Jersey Institute of Technology (NJIT), USA, in 2013. He has seven granted international patents, published six international patents, filed five international patents, four book chapters, and more than 30 publications. His research interests include the establishment of digital biotwin of human organs, biosignal processing, cardiac computational model, human performance and behavioral modeling, ontology, AI, personalized diagnosis systems, wearable devices, and medical device development.

He works on ECG for Person Identification and Authentication won the MIT TR35 (Young Innovator) 2011 Award from MIT Review India Edition. In the same year, another work on Portable Cardiac Devices won the Dare to Try TATA Innovista 2011 Award. In addition, World CSR Congress and World CSR Day recognized his work on ECG as a biometric system for individual identification as one of the 50 most socially impactful innovators (global listing), in 2016. He has chaired international conferences and workshops.